JOURNAL OF COMPUTATIONAL PHYSICS 10, 324–340 (1972)

# Calculating Three-Dimensional Flows around Structures and over Rough Terrain*

C. W. HIRT† AND J. L. COOK†

*University of California, Los Alamos Scientific Laboratory, Los Alamos, New Mexico 87544*

Received November 22, 1971

A computing technique for low-speed fluid dynamics has been developed for the calculation of three-dimensional flows in the vicinity of one or more block-type structures. The full time-dependent Navier–Stokes equations are solved with a finite-difference scheme based on the Marker-and-Cell method. Effects of thermal buoyancy are included in a Boussinesq approximation. Marker particles that convect with the flow can be used to generate streaklines for flow visualization, or they can diffuse while convecting to represent the dispersion by turbulence of particulate matter. The vast amount of data resulting from these calculations has been rendered more intelligible by perspective-view and stereo-view plots of selected velocity and marker-particle distributions.

## I. INTRODUCTION

Finite-difference solutions have been obtained for many complicated fluid-flow problems [1], but until recently, there have been relatively few of these involved with three-dimensional transient flows. The three-dimensional calculations that have been reported have been restricted in scope, having been developed for the solution of specific problems, for example, the structure of the planetary boundary layer [2], for Bénard convection [3], and for flow between two concentric cylinders [4]. In this paper a method is described for calculating transient three-dimensional flows about large obstacles and over irregular boundaries. The technique is based on a simple variant of the Marker-and-Cell method [5] for the solution of the incompressible Navier–Stokes equations. Thermal-buoyancy effects are included in a Boussinesq approximation, and a technique developed by Sklarew [6] is used to represent the convection and diffusion of particulate matter. Only confined flow calculations are reported here. Extensions to three-dimensional, free surface, flows over and around obstacles will be reported elsewhere [7].

A major problem with three-dimensional calculations is the limited numerical

* This work was performed under the auspices of the United States Atomic Energy Commission.

† Now at Science Applications, Inc., Box 2351, la Jolla, CA. 92037.

resolution that may be obtained with the fast access memories of even the largest computers. Of course, additional external storage devices may be employed but these usually require much larger amounts of computer time. The program used for the examples in this paper is limited to a maximum of 3375 computational cells when run on a CDC 7600 computer with a 64 000-word fast core memory. This is not large, since 3375 cells is equivalent to a cubical mesh with only 15 cells on an edge. Nevertheless, sample calculations show that meaningful and interesting calculations can be performed even with this limited resolution.

Another problem associated with three-dimensional calculations is how to reduce the vast amounts of computed data into easily assimilated forms. Displays of velocities, contours, and other kinds of data taken from two-dimensional slices through a three-dimensional mesh are not always sufficient to form a clear picture of the complete flow pattern. To reconstruct a composite three-dimensional mental picture from a collection of two-dimensional slices is not an easy task. An alternative and more efficient means of displaying data is described in this paper. The technique is based on a hidden-line perspective-view plot routine designed especially for finite-difference calculations [8]. A perspective picture of, for example, velocity vectors associated with a given two-dimensional plane of calculational cells shows not only the three-dimensional variations of the vectors, but also their orientation with respect to all nearby obstacles. An even better display method consists of making two perspective views from slightly different observation points. When correctly done the result can be combined into a stereoscopic view, which is the ideal way to see the structure of three-dimensional flows.

Examples of these various display methods are described in more detail in the text. In Section II a description of the basic fluid-dynamic computing technique is presented together with some of its properties. Section III contains descriptions of the buoyancy and particulate transport models.

## II. The Basic Technique

### A. *Finite-Difference Approximations*

The Marker-and-Cell technique for the calculation of incompressible fluid flow [5] is an Eulerian finite-difference approximation to the Navier–Stokes equations

$$\begin{aligned}
\frac{\partial u}{\partial t} + \frac{\partial u^2}{\partial x} + \frac{\partial uv}{\partial y} + \frac{\partial uw}{\partial z} &= -\frac{\partial p}{\partial x} + g_x + \nu\left(\frac{\partial^2 u}{\partial x^2} + \frac{\partial^2 u}{\partial y^2} + \frac{\partial^2 u}{\partial z^2}\right), \\
\frac{\partial v}{\partial t} + \frac{\partial vu}{\partial x} + \frac{\partial v^2}{\partial y} + \frac{\partial vw}{\partial z} &= -\frac{\partial p}{\partial y} + g_y + \nu\left(\frac{\partial^2 v}{\partial x^2} + \frac{\partial^2 v}{\partial y^2} + \frac{\partial^2 v}{\partial z^2}\right), \qquad (1) \\
\frac{\partial w}{\partial t} + \frac{\partial wu}{\partial x} + \frac{\partial wv}{\partial y} + \frac{\partial w^2}{\partial z} &= -\frac{\partial p}{\partial z} + g_z + \nu\left(\frac{\partial^2 w}{\partial x^2} + \frac{\partial^2 w}{\partial y^2} + \frac{\partial^2 w}{\partial z^2}\right),
\end{aligned}$$

and the mass equation

$$\frac{\partial u}{\partial x} + \frac{\partial v}{\partial y} + \frac{\partial w}{\partial z} = 0, \tag{2}$$

where $p$ is the ratio of pressure to constant density, $g_x$, $g_y$, $g_z$ are prescribed body accelerations and $\nu$ is the coefficient of kinematic viscosity. In addition to solving directly for the velocity components and pressures, the Marker-and-Cell method also uses marker particles that are convected about by the fluid to record the locations of free surfaces. In this paper only confined flows are considered so that marker particles are not required for this purpose, but they are used to represent distributions of particulate matter as described in Section III.B.

The region in which computations are to be performed is divided into a set of small rectangular cells having edge lengths $\delta x$, $\delta y$, and $\delta z$. With respect to this set of computational cells, velocity components are located at cell faces and pressure values are at cell centers, see Fig. 1. Cells are labeled with an index $(i, j, k)$, which denotes the cell number as counted from the origin in the $x$, $y$, and $z$ directions, respectively. Also $p_{i,j,k}$ is the pressure at the center of cell $(i, j, k)$, while $u_{i+1/2,j,k}$ is the $x$-direction velocity at the center of the face between cells $(i, j, k)$ and $(i + 1, j, k)$, and so on.

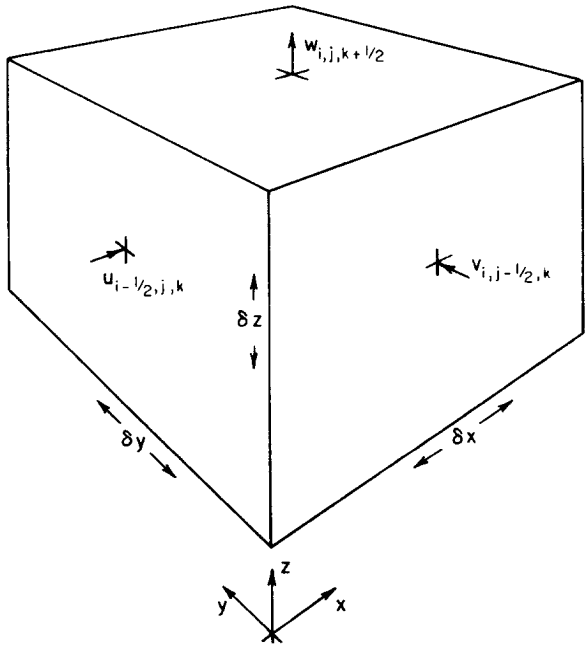


FIG. 1. Location of velocity components on a typical Eulerian cell $(i, j, k)$.

A time-dependent solution is obtained by advancing the flow field variables through a sequence of short time steps of duration $\delta t$. The advancement for one time step is calculated in two stages. First the velocity components are all advanced using the previous state of the flow to calculate the accelerations caused by convection, viscous stresses, body forces, pressure gradients, etc. In other words, stage one consists of a simple explicit calculation. However, this explicit time advancement does not necessarily lead to a velocity field with zero divergence, that is, to one that conserves mass. Thus, in stage two, adjustments must be made to insure mass conservation. This is done by adjusting the pressure in each cell in such a way that there is no net mass flow in or out of the cell. A change in one cell will affect neighboring cells so that this pressure adjustment must be performed iteratively until all cells have simultaneously achieved a zero mass change.

In the original Marker-and-Cell method the pressures in stage two were obtained from the solution of a Poisson equation. A related technique developed by Chorin [3] involved a simultaneous iteration on pressures and velocity components. Viecelli [9] has shown that the two methods as applied to the Marker-and-Cell method are equivalent. In this paper we have chosen the second procedure and simultaneously iterate both pressures and velocities. This choice simplifies the applications of boundary conditions as discussed in Section II.C.

The specific finite-difference expressions used for the steps described above may assume many forms. Those that follow are essentially direct extensions of the original Marker-and-Cell method. The stage one, explicit advancement of velocities, resulting in quantities labeled by tildes, is

$$\begin{aligned}\tilde{u}_{i+1/2,j,k} = u_{i+1/2,j,k} &+ \delta t\{(1/\delta x)[(u_{i,j,k})^2 - (u_{i+1,j,k})^2] \\ &+ (1/\delta y)[(uv)_{i+1/2,j-1/2,k} - (uv)_{i+1/2,j+1/2,k}] + (1/\delta z)[(uw)_{i+1/2,j,k-1/2} \\ &- (uw)_{i+1/2,j,k+1/2}] + g_x + (1/\delta x)(p_{i,j,k} - p_{i+1,j,k}) \\ &+ (\nu/\delta x^2)(u_{i+3/2,j,k} - 2u_{i+1/2,j,k} + u_{i-1/2,j,k}) \\ &+ (\nu/\delta y^2)(u_{i+1/2,j+1,k} - 2u_{i+1/2,j,k} + u_{i+1/2,j-1,k}) \\ &+ (\nu/\delta z^2)(u_{i+1/2,j,k+1} - 2u_{i+1/2,j,k} + u_{i+1/2,j,k-1})\},\end{aligned}$$

$$\begin{aligned}\tilde{v}_{i,j+1/2,k} = v_{i,j+1/2,k} &+ \delta t\{(1/\delta x)[(vu)_{i-1/2,j+1/2,k} - (vu)_{i+1/2,j+1/2,k}] \\ &+ (1/\delta y)[(v_{i,j,k})^2 - (v_{i,j+1,k})^2] \\ &+ (1/\delta z)[(vw)_{i,j+1/2,k-1/2} - (vw)_{i,j+1/2,k+1/2}] \\ &+ g_y + (1/\delta y)(p_{i,j,k} - p_{i,j+1,k}) \\ &+ (\nu/\delta x^2)(v_{i+1,j+1/2,k} - 2v_{i,j+1/2,k} + v_{i-1,j+1/2,k}) \\ &+ (\nu/\partial y^2)(v_{i,j+3/2,k} - 2v_{i,j+1/2,k} + v_{i,j-1/2,k}) \\ &+ (\nu/\delta z^2)(v_{i,j+1/2,k+1} - 2v_{i,j+1/2,k} + v_{i,j+1/2,k-1})\},\end{aligned}$$

$$\tilde{w}_{i,j,k+1/2} = w_{i,j,k+1/2} + \delta t\{(1/\delta x)[(wu)_{i-1/2,j,k+1/2} - (wu)_{i+1/2,j,k+1/2}]$$
$$+ (1/\delta y)[(wv)_{i,j-1/2,k+1/2} - (wv)_{i,j+1/2,k+1/2}]$$
$$+ (1/\delta z)[(w_{i,j,k})^2 - (w_{i,j,k+1})^2]$$
$$+ g_z + (1/\delta z)(p_{i,j,k} - p_{i,j,k+1})$$
$$+ (\nu/\delta x^2)(w_{i+1,j,k+1/2} - 2w_{i,j,k+1/2} + w_{i-1,j,k+1/2})$$
$$+ (\nu/\delta y^2)(w_{i,j+1,k+1/2} - 2w_{i,j,k+1/2} + w_{i,j-1,k+1/2})$$
$$+ (\nu/\delta z^2)(w_{i,j,k+3/2} - 2w_{i,j,k+1/2} + w_{i,j,k-1/2})\}. \tag{3}$$

Quantities needed at positions other than where they are defined are calculated as simple averages, e.g., $u_{i,j,k} = \frac{1}{2}(u_{i+1/2,j,k} + u_{i-1/2,j,k})$, and the square of a quantity, e.g., $u^2$ at $(i, j, k)$ is the square of the average, $(u_{i,j,k})^2$, rather than the average of the squares, $u^2_{i+1/2,j,k}$ and $u^2_{i-1/2,j,k}$.

The computations indicated in (3) are made for all $(i, j, k)$, and represent a straightforward explicit finite-difference approximation to (1). Although centered differences have been used in approximating the convection terms, the resulting equations will be stable provided sufficient viscosity is applied. This is similar to the MAC method [10], and is more fully described in Section II.E.

## B. *Pressure Iteration*

Equations (3) do not necessarily result in a velocity field that satisfies (2), so that some adjustment of the tilde velocities must be made to insure mass conservation. An iterative process is used for this purpose, in which the cell pressures are modified to make the velocity divergence vanish. In each cell $(i, j, k)$ the value of the velocity divergence $D$ is calculated as

$$D_{i,j,k} = (1/\delta x)(u_{i+1/2,j,k} - u_{i-1/2,j,k}) + (1/\delta y)(v_{i,j+1/2,k} - v_{i,j-1/2,k})$$
$$+ (1/\delta z)(w_{i,j,k+1/2} - w_{i,j,k-1/2}). \tag{4}$$

If the magnitude of $D$ is less than some prescribed small value $\epsilon$, the flow is locally incompressible and no change in the cell velocity is necessary. However, if the magnitude of $D$ is larger than $\epsilon$ then the pressure is changed by

$$\delta p = -\beta D, \tag{5}$$

where $\beta$ is given by

$$\beta = \beta_0/2\delta t \left(\frac{1}{\delta x^2} + \frac{1}{\delta y^2} + \frac{1}{\delta z^2}\right). \tag{6}$$

The constant $\beta_0$ is a relaxation factor, where overrelaxation and underrelaxation correspond to $\beta_0$ greater than or less than unity, respectively. For iteration stability

it is necessary to keep $\beta_0 < 2$. A value of $\beta_0 \approx 1.7$ is commonly used, but this is occasionally too large when there are strong flow distortions. The value of $\beta_0$ giving the most rapid convergence can, in general, only be determined by experimentation.

Once $\delta p$ has been calculated for a cell $(i, j, k)$ it is necessary to add it to the pressure $p_{i,j,k}$, and to adjust the velocity components on the sides of cell $(i, j, k)$ according to.

$$
\begin{aligned}
u_{i+1/2,j,k} &\rightarrow u_{i+1/2,j,k} + (\delta t/\delta x)\,\delta p,\\
u_{i-1/2,j,k} &\rightarrow u_{i-1/2,j,k} - (\delta t/\delta x)\,\delta p,\\
v_{i,j+1/2,k} &\rightarrow v_{i,j+1/2,k} + (\delta t/\delta y)\,\delta p,\\
v_{i,j-1/2,k} &\rightarrow v_{i,j-1/2,k} - (\delta t/\delta y)\,\delta p,\\
w_{i,j,k+1/2} &\rightarrow w_{i,j,k+1/2} + (\delta t/\delta z)\,\delta p,\\
w_{i,j,k-1/2} &\rightarrow w_{i,j,k-1/2} - (\delta t/\delta z)\,\delta p.
\end{aligned} \tag{7}
$$

This process is repeated successively in all cells until no cell has a magnitude of $D$ greater than $\epsilon$.

With the proper application of boundary conditions the pressure iteration will converge, and it will do so in relatively few sweeps of the mesh, provided the flow is not changing too rapidly from one cycle to the next, and provided $\epsilon$ is not chosen excessively small. For the problems illustrating this paper approximately 5–10 sweeps are necessary with an $\epsilon$ typically of magnitude $10^{-2}U/L$, where $U/L$ is a representative velocity to length ratio.

When the iteration has converged, the adjusted velocities satisfy the mass-conservation condition (2), and this completes the necessary calculations for advancing the flow field through one cycle in time.

If, in addition, it is desired to permit the transport of heat or pollution concentrations these field quantities must also be advanced one time step before beginning the next fluid-dynamic cycle. Likewise, discrete marker particles used to define particulate distributions, or for flow-visualization purposes, must be moved before starting the next cycle.

### C. *Boundary Conditions*

The five principle kinds of boundary conditions to be considered are rigid free-slip walls, rigid no-slip walls, inflow and outflow boundaries, and periodic boundaries. For simplicity it will be assumed that all physical boundaries coincide with cell boundaries. The inclusion of more general boundary configurations is a difficult problem, but a good start in this direction for two-dimensional flows has been made by Viecelli [9].

The prescription of boundary conditions consists of a choice for both the normal

and tangential velocities at the boundary. The normal velocity is easy to prescribe when the boundary coincides with a cell edge, since it is the normal velocity that is stored for each cell face. For a rigid boundary this velocity is set to zero, while for an input boundary it is assigned the desired input value. If the boundary is periodic the value must be chosen equal to the corresponding velocity one wavelength away. For outflow boundaries, however, there is no unique prescription, but the general idea is to chose boundary conditions that have the least upstream influence. It has been found that for this purpose a useful prescription consists of setting the normal *tilde* velocity on the outflow boundary equal to the corresponding *tilde* velocity immediately upstream, and then letting the velocity on the boundary relax as it wishes during the pressure iteration. This appears to keep the flow going smoothly out of the boundary in the examples tested.

Tangential velocities are needed in cells immediately outside the fluid region in order to specify the appropriate viscous stress at the boundary. These velocities are set equal to the adjacent velocities inside the fluid when it is desired that the boundary represent a free-slip wall (plane of symmetry), and they are set equal to the negative of the adjacent fluid velocities when the boundary is to be no slip. In other words, the external velocities tangent to a boundary are chosen to give either vanishing shear or vanishing velocity at a rigid wall. A more complete discussion of these alternatives and the conditions under which each should be used is contained in Ref. [11]. If the boundary is periodic then these external velocities are set equal to their counterparts one wavelength away, and at an inflow boundary they are prescribed to give the desired input flow. At an outflow boundary they are set equal to the adjacent velocities inside the fluid, which encourages a smooth transition through the outflow boundary.

To aid in the identification of various kinds of boundaries a flagging scheme is employed in the computer program, which assigns to each cell a number that identifies it as an obstacle cell, inflow cell, outflow cell, etc. In this way it is easy to arrange a distribution of obstacles in a mesh, and to have various combinations of inflow and outflow boundaries.

Several examples illustrating different combinations of boundary conditions are shown in Figs. 2–6. In Fig. 2 a horizontal layer of velocity vectors is shown in perspective for steady flow around a simple rectangular structure. A uniform flow is entering the computing region (large rectangular box) through the left face and is leaving through the right face. Each vector (short line segment) is drawn from the corner of a computing cell with a direction and magnitude representing the average velocity about that corner.

A recirculation in the wake region is clearly evident in the figures. It consists of a pair of counter-rotating eddies that are small near the top of the structure, but large near its base. The $x$–$y$ components of the same set of velocity vectors have been plotted in Fig. 3. Here the double eddy structure is more clearly seen, but no

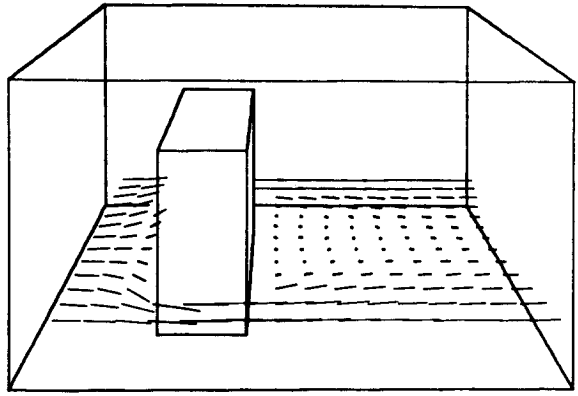

FIG. 2. Perspective view of velocity field about a single building.

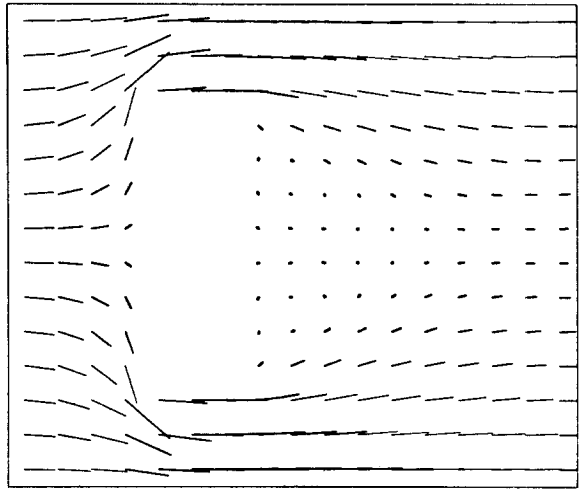

FIG. 3. Projection of velocity vectors seen in Fig. 2 on a $z$ = const. plane.

indication of the distribution of $z$-component velocity is available in this kind of plot. Velocity vectors for a similar calculation, but involving a more complicated obstacle, are shown in Figs. 4–5. The three dimensionality of the velocities is most clearly seen in Fig. 5.

In the previous examples the inflow is normal to the front face of the obstacle, but by making two adjacent sides of the mesh inflow boundaries and the opposite two sides outflow boundaries, the incident flow can be adjusted to any angle. Figure 6, for example, shows the results of a calculation with the flow passing

through the mesh from left to right, and oriented 45° to the large faces of the two obstacles.

### D. *Computer Requirements*

In the previously described calculations the total number of computational cells used was 3344, requiring an average calculation time of 1–2 sec per time cycle on a CDC 7600 computer. With this number of cells the computer program absorbed nearly all the storage available in a 64 000-word fast core memory. Fortunately, even with this limited resolution there are many interesting calculations that can be performed.

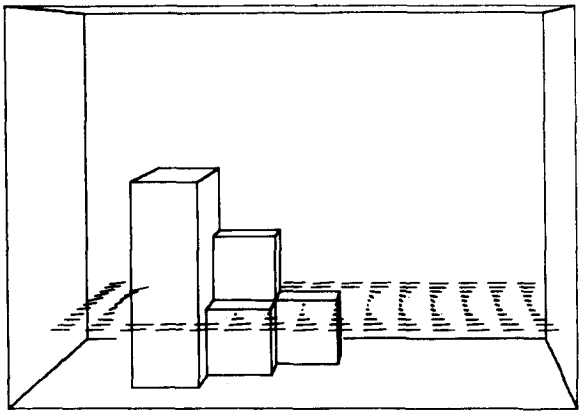

FIG. 4. Perspective view of velocity field near the bottom of a complicated structure.

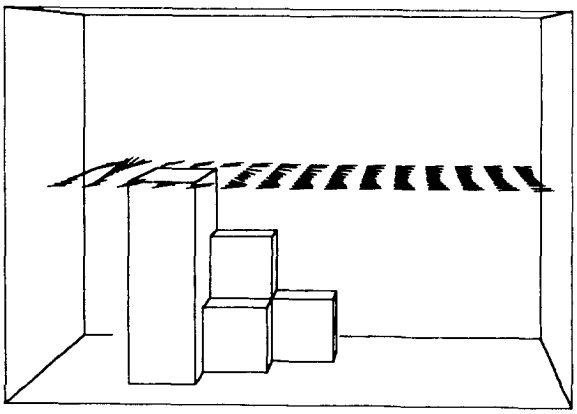

FIG. 5. Perspective view of velocity field near the top of a complicated structure.

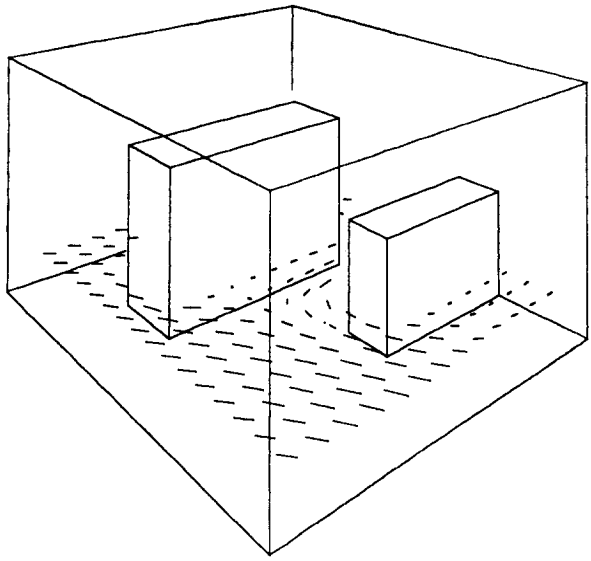

FIG. 6. Perspective view of velocity field in vicinity of two buildings. Incident flow is oriented 45° with respect to large faces of the buildings.

The problem of what to do when more resolution is needed, however, is an interesting one that deserves further comment. Clearly, the simplest approach is to use auxiliary memory units. Although more computer time is needed when operating with this kind of storage, because of the longer time needed to retrieve data, the calculation time for the examples illustrating this paper could easily be increased by an order of magnitude without becoming too unreasonable. An order of magnitude increase is roughly equivalent to doubling the finite-difference resolution, since that requires a factor of eight increase in the number of cells and a somewhat larger increase in calculation time.

Nevertheless, it is easy to think of three-dimensional problems in which still larger increases in resolution are required, and aside from relying on the development of larger and faster computers, it is clear that more effort must be devoted to improving both computer-programming and numerical-approximation methods.

### E. *Numerical Stability*

No additional stability conditions are introduced in the Marker-and-Cell method when it is used for three-dimensional computations, but the stability conditions previously reported [5, 10, 12] must be appropriately modified.

The basic restriction on the size of the time step $\delta t$ is that fluid must not be

permitted to flow across more than one computational cell in one time step, that is,

$$\delta t < \min[\delta x/|\, u\,|\,,\ \delta y/|\, v\,|\,,\ \delta z/|\, w\,|]. \tag{8}$$

This is clearly a numerical accuracy condition, because the convective flux approximations used in the tilde calculations (3) assume exchanges between adjacent cells only. This condition must also be satisfied for numerical stability, as can be verified by linearizing the difference equations and performing a Fourier analysis on them [12].

The linear analysis also reveals that the equations will always be unstable unless the kinematic viscosity $\nu$ is large enough; a good approximation is

$$\nu > (\delta t/2)\max[u^2, v^2, w^2]. \tag{9}$$

This condition follows easily from a heuristic stability analysis [10], which shows that $\nu$ should also satisfy the following approximate inequality,

$$\nu > \max\left[\tfrac{1}{2}\delta x^2 \left|\frac{\partial u}{\partial x}\right|,\ \tfrac{1}{2}\delta y^2 \left|\frac{\partial v}{\partial y}\right|,\ \tfrac{1}{2}\delta z^2 \left|\frac{\partial w}{\partial z}\right|\right]. \tag{10}$$

The last two conditions imply a lower bound on the kinematic viscosity, which imposes an upper limit on the flow Reynolds number. This Reynolds-number restriction is not unique to the Marker-and-Cell method, but is a necessary feature of all finite-difference methods. The reasons for this can be shown in many ways. One way is to argue as follows: Truncation errors are unavoidable in finite-difference approximations, and even though they do not always lead to instabilities that require restrictions like (9) or (10), they do influence the accuracy of a calculation. For purposes of accuracy, if the effects of $\nu$ are not to be obscured by truncation errors it is necessary that

$$\nu > \alpha \Delta x \Delta u, \tag{11}$$

where $\alpha$ is some numerical factor of order unity, $\Delta x$ is a typical cell dimension, and $\Delta u$ is a typical velocity change across a cell. This relation is based on the observation that a difference approximation of order $(p + 1)$ will have truncation error terms that modify $\nu$ by a contribution like,

$$\delta x^{p+1}(\partial^p u/\partial x^p).$$

In a finite-difference approximation this quantity will be approximated by $\alpha \Delta x \Delta u$, which defines the value of $\alpha$. For the order of magnitude estimate wanted here, $\alpha$ can be replaced by unity. Thus, (11) is simply the statement that $\nu$ must be larger than these errors for an accurate calculation. Now if a typical dimension in a flow $L$ is resolved by $N$ finite-difference cells, $L = N\Delta x$, and if a typical velocity $U$ is

$N\Delta u$, then (11) also states that the flow Reynolds number, $R \equiv UL/\nu$, must be less than $N^2$. In other words, the condition

$$R < N^2 \tag{12}$$

is a necessary restriction for accurate finite-difference calculations.

It may be noted that a few finite-difference approximations, for example, those using the so-called donor-cell approximation [13], have even larger truncation errors that lead to the more restrictive condition

$$R < N. \tag{12a}$$

Condition (12) is a rough estimate for the maximum allowable Reynolds number obtainable with any finite-difference approximation. It is primarily an accuracy condition, but it often happens, as in the present case, that it is a condition for stability as well.

Finally, when very low Reynolds-number flows are to be simulated the time step is additionally restricted by the condition

$$\nu\delta t < 1/2\left(\frac{1}{\delta x^2} + \frac{1}{\delta y^2} + \frac{1}{\delta z^2}\right). \tag{13}$$

In analogy with the interpretation of (8) this restriction may be roughly described as limiting the distance over which momentum diffuses during one time step to be less than one cell width.

## III. Auxiliary Features

### A. *Thermal Buoyancy*

A heat equation may be simultaneously solved with the fluid equations in order to similate the effects of thermal buoyancy that are important for many meteorological applications. The differential equation governing convection and diffusion of temperature $T$ is

$$(\partial T/\partial t) + \nabla \cdot T\mathbf{u} = \nabla \cdot (\lambda \nabla T), \tag{14}$$

where $\lambda$ may be chosen to represent both turbulent and molecular diffusion processes. The finite-difference expression used to approximate (14) assumes that $T_{i,j,k}$ is located at the center of cell $(i, j, k)$,

$$\begin{aligned} T_{i,j,k}^{n+1} = T_{i,j,k} &+ \delta t\{(1/\delta x)[\langle Tu\rangle_{i-1/2,j,k} - \langle Tu\rangle_{i+1/2,j,k}] \\ &+ (1/\delta y)[\langle Tv\rangle_{i,j-1/2,k} - \langle Tv\rangle_{i,j+1/2,k}] \\ &+ (1/\delta z)[\langle Tw\rangle_{i,j,k-1/2} - \langle Tw\rangle_{i,j,k+1/2}] \\ &+ \lambda[(1/\delta x^2)(T_{i+1,j,k} - 2T_{i,j,k} + T_{i-1,j,k}) \\ &+ (1/\delta y^2)(T_{i,j+1,k} - 2T_{i,j,k} + T_{i,j-1,k}) \\ &+ (1/\delta z^2)(T_{i,j,k+1} - 2T_{i,j,k} + T_{i,j,k-1})]\}. \end{aligned} \tag{15}$$

A constant diffusion coefficient has been assumed for simplicity, but this can be easily changed. The notation $\langle Tu \rangle_{i+1/2,j,k}$ means that the flux between cell $(i, j, k)$ and $(i + 1, j, k)$ is to be evaluated by the donor-cell rule [13], that is,

$$\langle Tu \rangle_{i+1/2,j,k} = \begin{cases} T_{i,j,k} u_{i+1/2,j,k}, & \text{if } u_{i+1/2,j,k} \geqslant 0 \\ T_{i+1,j,k} u_{i+1/2,j,k}, & \text{if } u_{i+1/2,j,k} < 0. \end{cases}$$

Donor-cell fluxes are used here to insure numerical stability and to avoid negative temperatures upstream from a local hot spot.

The most common boundary condition on the temperature is that of zero flux, which corresponds to a nonconducting wall or a plane of symmetry. Heat sources can be added in a variety of ways. Either selected portions of the boundaries can be given prescribed temperatures, or prescribed energy fluxes, or, energy can be deposited directly into selected regions of the fluid.

The effects of temperature variation are assumed to influence the fluid motions through a Boussinesq approximation, which consists of the addition of buoyancy terms to the right sides of the tilde equations (3). For example, the following term is added to the $w$-tilde equation,

$$\beta g_z (T_0 - T_{i,j,k+1/2}).$$

The constant $T_0$ is an initial reference temperature and $\beta$ is the coefficient of thermal expansion. This term requires a temperature at the boundary between two cells, which is equal to the average of the two cell temperatures.

An additional numerical stability condition is needed when Eq. (15) is used. This condition, which is analagous to (13), is

$$\lambda \delta t < 1/2 \left( \frac{1}{\delta x^2} + \frac{1}{\delta y^2} + \frac{1}{\delta z^2} \right). \tag{16}$$

The temperature equation can also be used to represent the transport of particulate matter when temperature effects are not of interest, in which case $T$ is interpreted as the particulate concentration. For example, Fig. 7 shows a particulate distribution calculated in this way (with $\beta$ equal to zero). The air flow is incident at 45° to the buildings, as shown in Fig. 6. There is a constant source of particulate matter being inserted at the center of the base of the large obstacle on the side furthest from view. The particulate concentration is shown in Fig. 7 as a distribution of particles. This was made by plotting in each cell a number of particles proportional to the cell concentration $T$, and with positions distributed randomly within the cell.

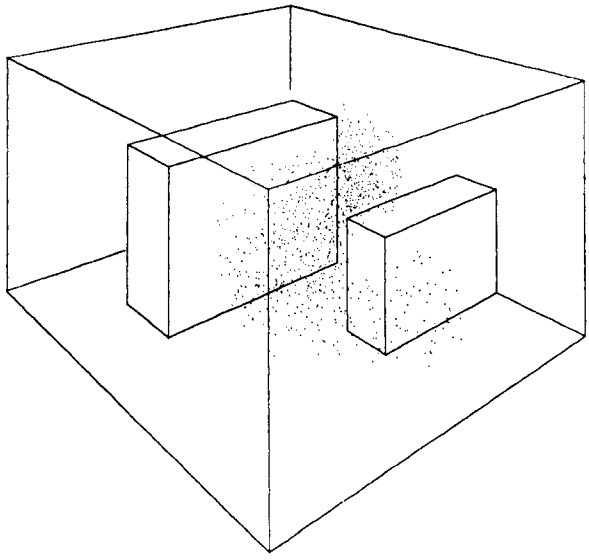

FIG. 7. Perspective view of particulate distribution in flow field shown in Fig. 6.

B. *Marker Particles*

The above technique for particulate transport is not very refined and does not work well for problems having sharply defined regions of particulate matter. A better technique has been devised by R. C. Sklarew [6]. He keeps track of individual particles and uses a clever trick to move them so that their distribution represents a solution of (14). The trick is to rewrite this equation as

$$(\partial T/\partial t) + \nabla \cdot [\mathbf{u} - (\lambda/T)\nabla T]\, T = 0. \tag{17}$$

Now it is evident that if particles are moved (convected) with the effective velocity

$$\mathbf{u} - (\lambda/T)\nabla T, \tag{18}$$

they will approximate a solution of (17). Another way to say this is that the total flux of $T$ resulting from convection and diffusion is equivalent to a pure convection with the velocity (18). The concentration $T$ in a cell is then proportional to the number of marker particles in the cell. The diffusion coefficient can vary arbitrarily in space and time, and the method is stable provided no particle moves more than one cell width in one time step.

Figure 8 shows an application of the Sklarew method to the flow of a slowly dispersing plume passing over the top of a rectangular structure. The flow is the

same as that shown in Figs. 2–3. Particles are seen trapped and recirculated in the wake region.

A similar calculation is shown in Fig. 9 for a more complex building and with particulates emitted from a vent centrally located on top of the principle structure. The flow field for this problem is identical to that of Figs 4–5.

The numerical prescription used for moving particles is based on a straightforward extension of the technique used in the original Marker-and-Cell method

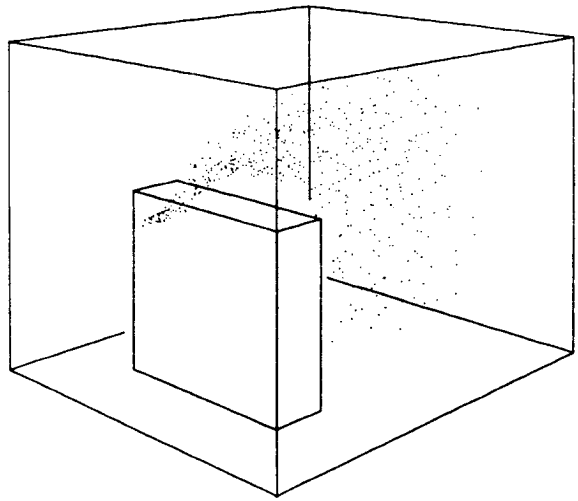

FIG. 8. The dispersal of a narrow plume passing over a single building. Recirculation in wake region is clearly evident.

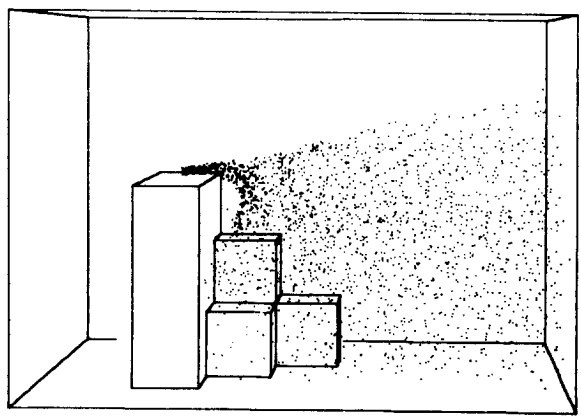

FIG. 9. The dispersal of pollutant from a flush vent on the top of a complex building structure.

[5]. Each particle is moved with a velocity obtained from a linear interpolation among the eight nearest cell velocities. The same interpolation is used whether the particles are to move with the fluid or with the effective velocity (18).

The only difficult problem in moving particles is to account for the presence of various boundary conditions. In the examples shown here, this has been accomplished by suitably adjusting the velocity interpolation factors when particles are near a boundary.

### C. *Data Display Techniques*

Most of the figures have displayed data in the form of perspective views. These views give a much better picture of the three-dimensional flow fields than could be obtained from sets of purely two-dimensional plots. In addition to the velocity vectors and particle distributions shown, it can be useful to plot perspective views of contour lines, streak lines, and, in general, anything having a three-dimensional distribution.

The perspective plots used here [8] have been designed especially for three-dimensional finite-difference calculations. They are so efficient that movies of transient flow phenomena can be made at little additional expense to a calculation. Movies can also be made with the observation point continually changing position, to give an even better feel for the three dimensionality of a problem.

Stereo pictures of velocity vectors and particle distributions have proven themselves to be extremely useful, but unfortunately they are not easily presented in journal articles. The usual procedure is to print, side by side, two perspective views made from slightly shifted observation points, as in Fig. 10(A). The left view

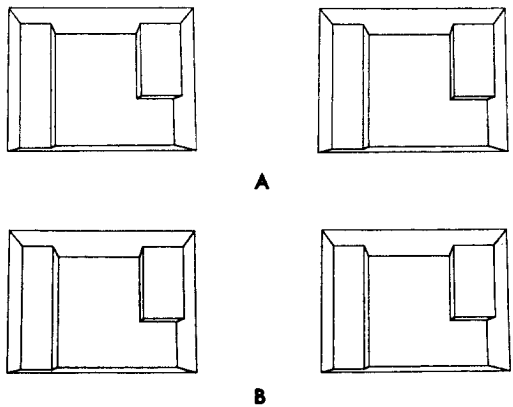


FIG. 10. The two perspective views in (A) appear in stero when viewed "walleyed," while those in (B) appear in stero when viewed "crosseyed."

is the correct perspective for the left eye and the right view is correct for the right eye. To see in stereo it is necessary to hold the figure approximately 18 in. in front of the eyes and to let the eyes move apart so that the combined eye images merge together at some distance beyond the page. Unfortunately, many persons cannot keep their eyes in focus while forcing them to move apart (walleyed). On the other hand, a large fraction of these people can keep them focused when they are moved together (crossed). Thus, in Fig. 10B the left and right images shown in Fig. 10(A) have been reversed. This figure will appear in stereo when the eyes are crossed to bring the images together at a point in front of the page. Admittedly it takes some practice to get a stereo view in either case, but the results are generally worth the effort.

## ACKNOWLEDGMENT

The authors would like to express their appreciation to Robert Hotchkiss who has supplied many valuable additions to the program, and who performed the calculations illustrated in Figs. 8–10.

## REFERENCES

1. F. H. HARLOW, "Numerical Methods for Fluid Dynamics — An Annotated Bibliography," Los Alamos Scientific Laboratory Report LA-4281 (1969).
2. J. W. DEARDORFF, *Geophys. Fluid Dynamics* **1** (1970), 377; *J. Fluid Mech.* **41** (1970), 453.
3. A. J. CHORIN, AEC Research and Development Report, NYO-1480-61 (1966).
4. G. P. WILLIAMS, *J. Fluid Mech.* **37** (1969), 727.
5. F. H. HARLOW AND J. E. WELCH, *Phys. Fluids* **8** (1965), 2182; J. E. WELCH, F. H. HARLOW, J. P. SHANNON, AND B. J. DALY, Los Alamos Scientific Laboratory Report, LA-3425 (1966).
6. R. C. SKLAREW, Paper presented at 63rd Annual Meeting Air Pollution Control Association, St. Louis, Missouri, June, 1970.
7. B. D. NICHOLS AND C. W. HIRT, in preparation.
8. C. W. HIRT AND J. L. COOK, in preparation.
9. J. A. VIECELLI, *J. Comput. Phys.* **8** (1971), 119.
10. C. W. HIRT, *J. Comput. Phys.* **2** (1968), 339.
11. B. D. NICHOLS AND C. W. HIRT, *J. Comput. Phys.*, to appear.
12. B. J. DALY AND W. E. PRACHT, *Phys. Fluids* **11** (1968), 15.
13. R. A. GENTRY, R. E. MARTIN, AND B. J. DALY, *J. Comput. Phys.* **1** (1966), 87.